

## DEVELOPMENT OF A STATISTICAL STRONG-MOTION EVALUATION METHOD CONSIDERING REGIONAL VARIATION OF SOURCE AND PATH EFFECTS IN THE TOHOKU REGION, JAPAN

S. Ohno<sup>1</sup>

<sup>1</sup> Associate Professor, Disaster Control Research Center, Tohoku University, Sendai, Japan  
Email: ohnos@archi.tohoku.ac.jp

### ABSTRACT :

A ground motion prediction equation for strong motion spectra is empirically developed for the Tohoku region, Japan. Spectral inversion analyses of S-wave Fourier spectra and 5% damped response spectra of identical datasets are conducted. Based on the results of the spectral inversion, PGA, PGV and response spectrum are modeled as a function of moment magnitude, stress drop, distance with three types of Q, and Vs30. It is found that the variance of the source term is significantly decreased by adding stress drop as a parameter. This indicates that taking into account regional variations of source radiation strength is effective to reduce the uncertainty in strong motion evaluation.

**KEYWORDS:** spectral inversion, ground motion prediction equation, Tohoku region, Japan

### 1. INTRODUCTION

Empirical attenuation relationship or ground motion prediction equation (GMPE) has been widely used to estimate ground motion intensities (PGA, PGV, response spectrum). Although it is difficult to take into account effects of complex phenomena such as detailed faulting process or basin-induced surface waves, the method is widely used for making seismic hazard maps because of its stability and easiness to apply. On the other hand, the studies of spectral inversion analysis have shown that the source spectral shapes and attenuation characteristics have strong regional variations (e.g., Satoh and Tatsumi, 2002). Recently new factors such as short-period level (Kataoka et al., 2006) and distance from volcanic front to represent anomalous seismic intensity due to subducting plate (Takai and Okada, 2002, Morikawa et al., 2006) are introduced in GMPE to improve its applicability. In this paper, spectral inversion analyses of Fourier and response spectra for identical dataset of strong motions are conducted. Base on these results, a GMPE is developed by considering regional variation of Q and source spectra for the Tohoku region, Japan.

### 2. DATA

Datasets used in this paper is records of the K-NET and KiK-net by DPRI, PARI, 87-type and 95-type JMA strong-motion networks. JMA magnitude and focal depth of the datasets range more than 5.0 and shallower than 100km, respectively. The period of the datasets is up to Aug. 2004, while the data of the recent disaster earthquakes of 10/23/2004 Niigata-ken-Chuetsu, 08/16/2005 Miyagi-ken-oki, 07/16/2006 Niigata-ken Chuetsu-oki are added. Figure 1 shows map of epicenters of the earthquakes. Triangles show shallow inland earthquakes and circles show earthquakes along with the pacific plate subducting under Japan Island from Japan Trench. The locations of the observation stations are shown in Fig.5.

Figure 2 shows relationships between moment-magnitude ( $M_W$ ) and equivalent hypocentral distance ( $X_{eq}$ , Ohno et al., 1993) of the datasets. Total of 119 earthquakes, 565 observation stations, 13003 records are used. Distances of the datasets are restricted within 100 km to avoid the effects of SmS or Lg waves for the inland earthquakes, and within 300km for the subduction earthquakes.  $X_{eq}$  is used to take into account the effect of fault extension. For major earthquakes in the datasets, the inhomogeneous slip distributions are used to calculate  $X_{eq}$ , otherwise hypocentral distance is used as  $X_{eq}$ . The number of records used for the inversion analysis depends on

frequency as shown in Fig.2(c), because low frequency noises are predominant in some records.

### 3. INVERSION ANALYSES OF FOURIER AND RESPONSE SPECTRA

The functional form used for the inversion analysis is given by Eqn.3.1.

$$\log O_{ij}(f) = \log S_i(f) - \log X_{eq_{ij}} + \delta_{ILi} b_{IL}(f) X_{eq_{ij}} + \delta_{Si} b_{SE}(f) XE_{ij} + \delta_{Si} b_{SW}(f) XW_{ij} + \log G_j(f) \quad (3.1)$$

$$XE = X_{eq} \cdot \Delta E / (\Delta E + \Delta W), XW = X_{eq} \cdot \Delta W / (\Delta E + \Delta W) \quad (3.2)$$

where log is logarithm (base 10),  $f$  is frequency, subscripts  $i, j$  indicate an earthquake and a site, respectively.  $O_{ij}(f)$  is either Fourier spectrum [cm/s] of S-wave portion, or PGA [cm/s<sup>2</sup>], PGV [cm/s], 5%-damped pseudo velocity response spectrum [cm/s] after S-wave arrival.  $X_{eq}$  [km] is equivalent hypocentral distance,  $XE$  [km] and  $XW$  [km] are forearc and backarc portions of source-to site distance to represent different attenuation characteristics between the forearc and backarc sides (Takai and Okada, 2002). In Eqn.3.2,  $\Delta E$  and  $\Delta W$  are the east and west portions of epicentral distance, divided at the volcanic front line in Fig.1.  $\delta_{ILi}$  takes 1 for inland earthquakes, 0 otherwise, and  $\delta_{Si}$  takes 1 for subduction earthquake, 0 otherwise.  $S_i(f), b_{IL}(f), b_{SE}(f), b_{SW}(f), G_j(f)$  are coefficients to be estimated by least-squares method. Vector sum of two horizontal components is used for Fourier spectrum and geometrical mean is used for the others.

For extracting S-wave portion from the records, time length  $T_L$  [s] of Eqn.3.4 is used as S-wave duration. Considering uncertainty due to rupture direction, Eqn.3.4 is given by 2.5s (minimum length of time window) plus twice of rupture duration  $T_W$  in Eqn.3.3.  $T_W$  is obtained from dividing rupture length  $L$ , a function of magnitude  $M$  (Sato, 1989), by assumed rupture velocity  $V_r$  of 3.0 km/s.

$$T_W = L/V_r = (0.5M - 1.88)/3.0 \approx 10^{0.5M-2.4} \quad (3.3)$$

$$T_L = 2.5 + 2T_W \quad (3.4)$$

The observed records at K-NET IWT009 and KiK-net FKSH07 (borehole) sites are converted to bedrock-outcropped motions using 1-D S-wave propagation theory with the substructure models proposed by Satoh and Tatsumi (2002) and JNES (2006), respectively. We selected these stations as the reference sites because 1) seismic bedrock ( $V_s$  of near 3km/s) is shallow (The  $V_s$  of bedrock are 2790 m/s at IWT009 and 2870 m/s at FKSH07), 2) reliable subsurface structure with damping factor is available, 3) reference points at both sides of volcanic front seems better to increase stability in the inversion analysis. The amplification factors at these reference sites are given as two, independent of frequencies. The locations of these reference stations are plotted in Fig.5(c).

#### 3.1 Quality Factor

Figure 3 shows the Q-values calculated by Eqn.3.5 from the estimates of  $b(f)$ .  $V_s$  of 3.6 km/s is used for  $b_{IL}$ ,  $V_s$  of 4.0 km/s is used for  $b_{SE}, b_{SW}$ , respectively.

$$Q(f) = -\log e \cdot \pi \cdot f \cdot b(f) / V_s \quad (3.5)$$

Approximately,  $100f^{1.0}$ ,  $180f^{0.7}$  and  $90f^{0.6}$  are obtained for the inland earthquakes, east and west of volcanic front for the subduction earthquakes, respectively. The Q-values estimated from Fourier and response spectra almost agree, while in the low frequencies there are some discrepancies. This difference is probably due to surface waves, because coda part is included for response spectral calculation, but not included for Fourier spectral calculation as described above.

#### 3.2 Site Amplification Factor

Figure 4 shows examples of the estimated site amplification factors  $G_j(f)$  for Fourier spectra at three KiK-net

sites, where  $V_s$  at borehole bottom ( $V_b$  in Fig.4) is relatively close to bedrock  $V_s$  at the reference sites. The locations of these stations are plotted in Fig.5(c). Figure 4 also plots theoretical amplification factors calculated by 1-D S-wave propagation theory, using PS logging profiles at the sites with assumed damping factor of  $7.5/V_s$  (m/s). The inversion results roughly agree with the theoretical amplifications.

Figure 5 shows maps of the amplification factors at 0.2Hz, 1Hz, and 5Hz with topography. The site amplification factors at 0.2 Hz and 1Hz are large in the major plains and basins indicated by allows. On the other hand, at 5Hz, the amplifications in the mountain regions become large compared with those in the plains. This is probably because shallow surface soft materials such as weathered rock overly hard rock in the mountain regions. Predominant frequency of such surface materials become high, as shown in the case of Fig.4(a).

### 3.3 Brune's Stress Drop (Stress Parameter)

Source spectrum  $M_{oi}(f)$  is calculated by Eqn.3.6 from the estimates of  $S_i(f)$ , under the condition that  $R_{\theta\phi} = 0.63$ ,  $\rho = 2.7 \text{ t/m}^3$  and  $3.0 \text{ t/m}^3$  for inland and subduction earthquakes, respectively. By fitting omega-square model of Eqn.3.7 to  $M_{oi}(f)$  using least-squares method, seismic moment  $M_o$  [Nm] and corner frequency  $f_c$  [Hz] are estimated, while only  $f_c$  is estimated when  $M_o$  is available from F-net or Harvard CMT solutions. Finally, Brune's stress drop  $\Delta\sigma$  [MPa] is calculated from Eqn.3.8.

$$M_{oi}(f) = (4\pi\rho V_s^3 / R_{\theta\phi}) S_i(f) \quad (3.6)$$

$$M_{oi}(f) = (2\pi f)^2 M_o / \{1 + (f/f_c)^2\} \quad (3.7)$$

$$\Delta\sigma = M_o f_c / (4.9 \times 10^6 V_s)^3 \quad (3.8)$$

Figure 6 shows relationships between the estimated stress drops and the moment magnitudes and the focal depths (centroid depth if available). The stress drops are widely scattered, especially in the small magnitude range. Also, general trend is seen that the stress drops of the deep earthquakes are averagely larger than those of the shallow earthquakes. Spatial distribution of the estimated stress drop is shown in Fig.1. From this figure, It is found that 1) the stress drops is very high off the east coast of Miyagi prefecture (around lat. 38, long. 142); 2) the stress drop is low for shallow inland earthquakes occurred near volcanoes; 3) inland earthquakes at other areas have stress drops similar to those of shallow earthquakes occurred in subduction zones.

## 4. MODELING OF RESPONSE SEPCTRUM

To make GMPE for PGA, PGV, and response spectrum, the estimated site amplification factor  $G(f)$  is modeled as a function of  $V_{s30}$  (averaged S-wave velocity from the ground surface to 30m depth), and earthquake term  $S(f)$  is modeled as a function of  $M_W$  and  $\Delta\sigma$ .

### 4.1 Site Amplification modeling by $V_{s30}$

The estimated site amplification factors of only K-NET and KiK-net stations are modeled as a function of  $V_{s30}$  because velocity profiles at the sites are provided for these networks. Figure 7 shows the amplification factors for PGA and PGV versus  $V_{s30}$ . The estimated amplification factors for PGA are widely scattered versus  $V_{s30}$ , while those for PGV show linear trend on  $V_{s30}$ . At first, the site amplification factors are modeled by Eqn.4.1, which has been widely used for modeling of site amplification (e.g. Midorikawa *et al.*, 1994).

$$\log G_j(f) = \alpha_1(f) \log(V_{s30_j}) + \beta(f) \quad (4.1)$$

$$\log G_j(f) = \alpha_2(f) \log(V_{s30_j} / V_{sb}) \quad (4.2)$$

The estimated coefficients with the standard deviations are shown in Fig.8. As shown in Fig.8(a),  $\alpha_1(f) \approx -1$  at frequencies less than about 2Hz, while  $\alpha_1(f)$  approaches zero as frequencies become higher. This frequency dependency on  $V_{s30}$  is similar as that of Kanno *et al.* (2006).

Eqn.4.2 has similar functional form as Eqn.4.1, except that  $\beta(f)$  become independent of frequency.  $V_{sb}$  of 1200 m/s is fixed based on the estimates of  $\beta(f)$  at frequencies less than 2 Hz. The estimated coefficient  $\alpha_2(f)$  nearly equals to  $\alpha_1(f)$  at less than 2 Hz, but show stronger dependence on  $V_{s30}$  at higher frequencies, while the standard deviations have similar values in both cases.

As one of the reasons of wide scattering in PGA and high frequency contents, high-frequency large amplifications at the mountain region, as shown in 3.2, is considered.  $V_{s30}$  may not be an appropriate index at high frequencies in application to sites where thin surface layer exist. Another possibility is the effect of nonlinear amplification of soils, which is not considered in this study. If the former is the major reason, Eqn.4.2 may give more appropriate results than Eqn.4.1 in this study.

#### 4.2 Earthquake term modeling by $M_w$ and $\Delta\sigma$

Figure 9 shows the earthquake terms for PGA and PGV versus  $M_w$ . If earthquake term  $S(f)$  follows omega-square model, the dependency of high-frequency level of  $S(f)$  on  $M_w$  and  $\Delta\sigma$  is expressed by Eqn.4.3. Base on this equation,  $S(f)$  is modeled as Eqn.4.4, where  $a_1(f)$ ,  $d(f)$ ,  $c_1(f)$  are coefficients to be estimated.  $S(f)$  is also modeled by Eqn.4.5 as the case that the parameter is magnitude only.

$$S_i(f) \propto M_o^{1/3} \Delta\sigma^{2/3} \propto 10^{0.5M_{wi}} \Delta\sigma^{2/3} \quad (4.3)$$

$$\log S_i(f) = a_1(f)M_{wi} + d(f)\log \Delta\sigma + c_1(f) \quad (4.4)$$

$$\log S_i(f) = a_2(f)M_{wi} + c_2(f) \quad (4.5)$$

The estimated coefficients with the standard deviations are shown in Fig.10. Fig.10(b) also plots the standard deviations for Eqn.3.1.  $a_1(f)$  and  $a_2(f)$ ,  $c_1(f)$  and  $c_2(f)$  have similar values, while  $a_1(f)$  show a little smaller dependence on  $M_w$ . Stress drop coefficient  $d(f)$  has larger value as frequencies become higher. The standard deviation for Eqn.4.4 is significantly decreased at high frequencies compared with that for Eqn.4.5. This indicates that the variations of  $S(f)$  shown in Fig.6 and Fig.9 are compensated well by Eqn.4.4.

#### 4.3 Ground Motion Prediction Equation for the Tohoku region, Japan

Based on the results described above, GMPE for the Tohoku region, Japan, is constructed by combining Eqns. 3.1 with 4.2 and 4.4. Figure 11 shows the application examples.  $\Delta\sigma$  of 10 Mpa in Eqn.4.4 gives similar results by Eqn.4.5.

## ACKNOWLEDGEMENTS

Strong motion records from DPRI, PARI, and JMA are used. This research was partially supported by Grant-in-Aid for Scientific Research (16560491) by Japan Society for the Promotion of Science. Figure 1 and Fig.5 are drawn by using the GMT software developed by Wessel and Smith (1991).

## REFERENCES

- JNES (2004) . <http://www4.jnes.go.jp/katsudou/seika/2004/kikaku/05kikou-0001.pdf>
- Kanno T., Narita, A., Morikawa, N., Fujiwara, H. and Y. Fukushima (2006). A New Attenuation Relation for Strong Ground Motion in Japan Based on Recorded Data, *Bull. Seism. Soc. Am.*, **96**, 879 -897.
- Kataoka, S., Satoh, T., Matsumoto, S. and Kusakabe, T. (2006) . Attenuation Relationships of Ground Motion Intensity using Short Period Level as a Variable, *Doboku Gakkai Ronbunshu A*, **62:4**, 740-757.
- Midorikawa, S., Matsuoka, M. and Sakugawa K. (1994). Site effects on strong-motion records observed during the 1987 Chiba-ken-toho-oki, Japan earthquake, *Proc. 9th Japan Earthquake Eng. Symposium*, E- 085-E-090.
- Morikawa, N., Kanno T., Narita, A., Fujiwara H. and Fukushima Y. (2006). New Additional Correction Terms for Attenuation Relations of Peak Amplitudes and Response Spectra Corresponding to the Anomalous Seismic Intensity in Northeastern Japan, *Journal of JAEE*, **6:1**, 23-41.

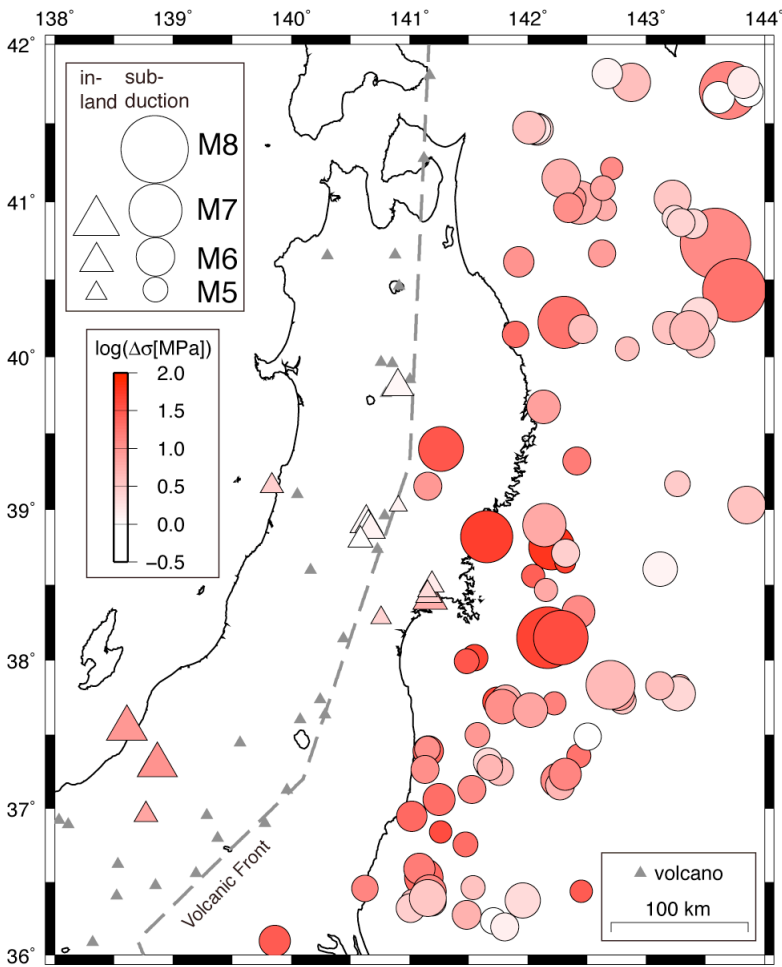


Figure 1 Map showing epicenter distribution of earthquakes with estimated stress drops. The volcanic front line is from Morikawa et al. (2006)

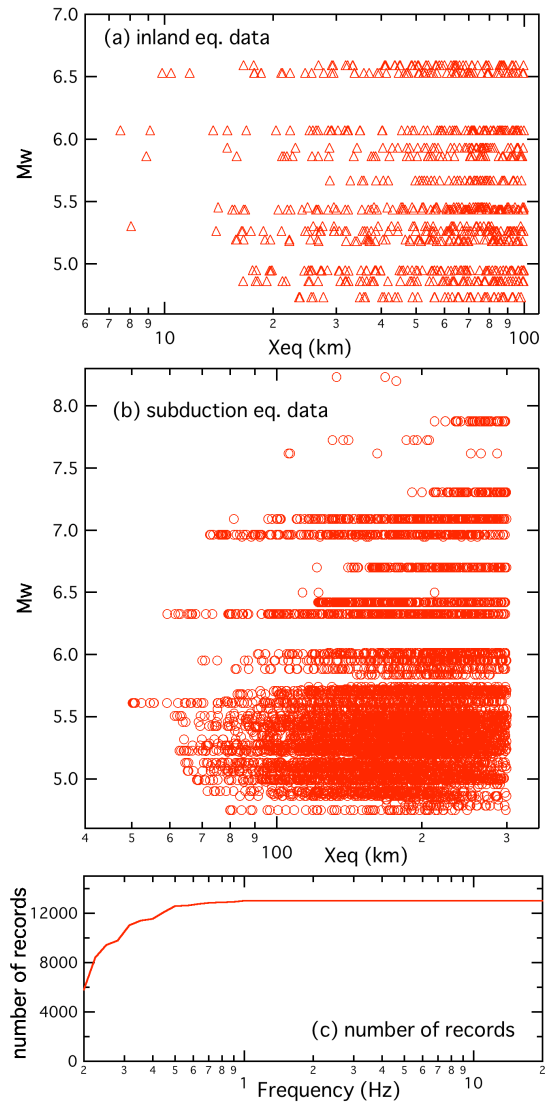


Figure 2 Magnitude-distance distributions of the data with frequency dependence of the data number

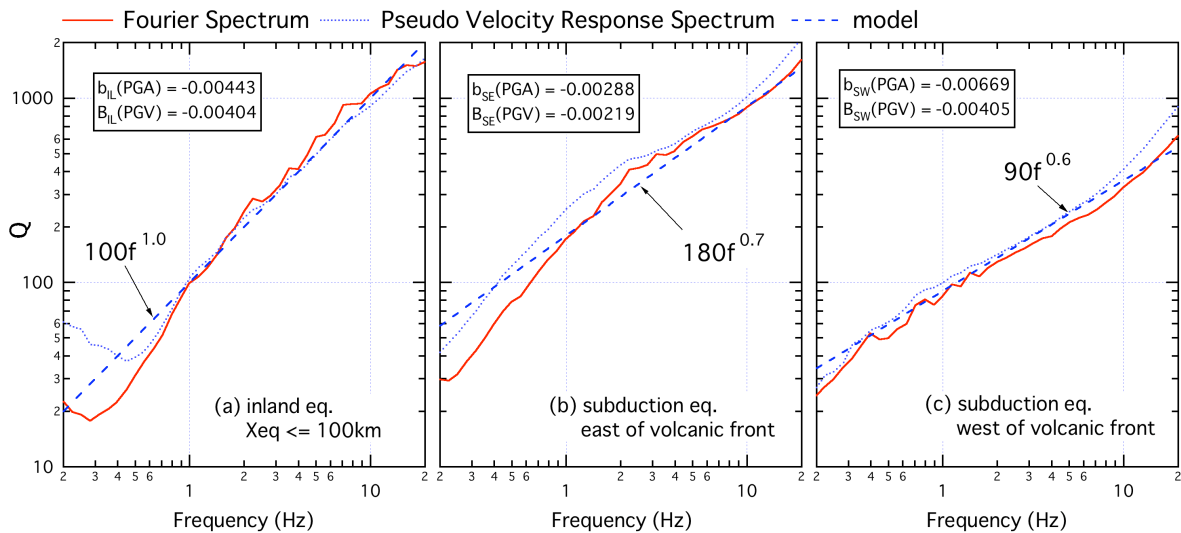


Figure 3 Estimated Q-values

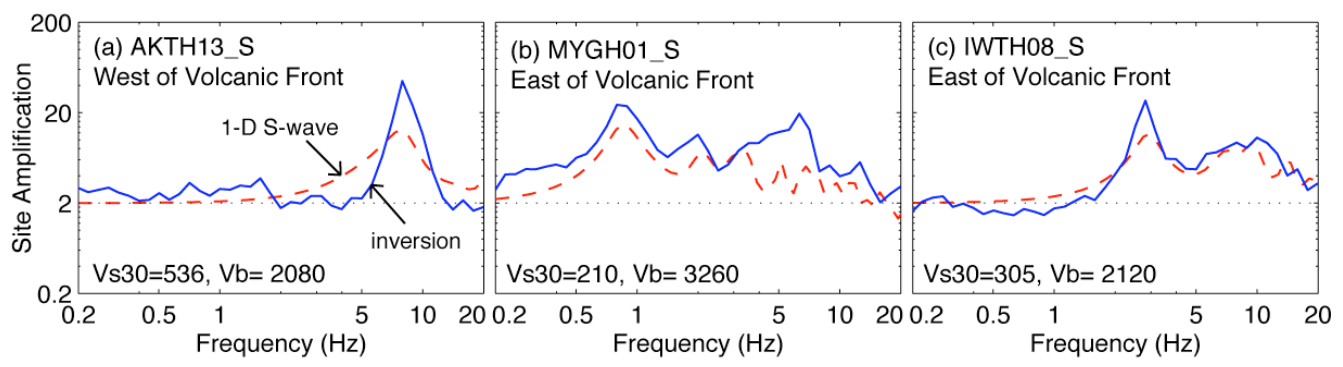


Figure 4 Examples of site amplification factors for Fourier spectra with 1-D S-wave theory

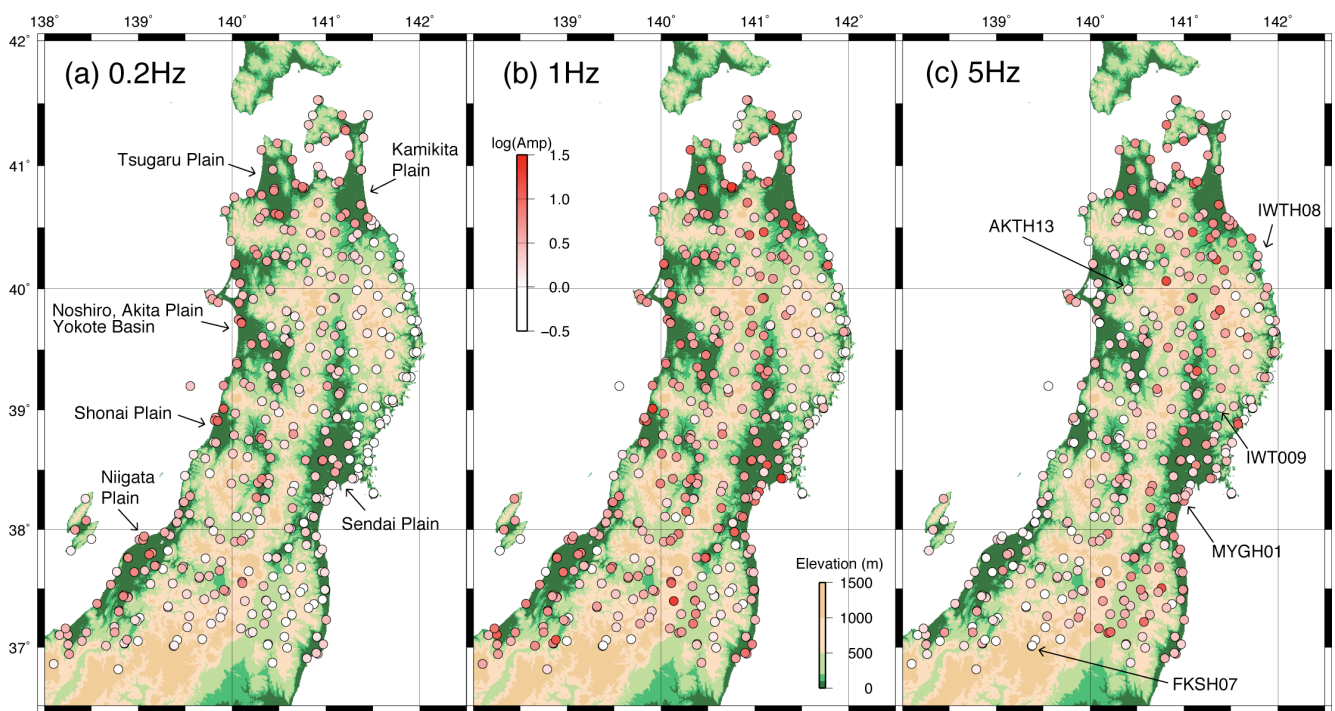


Figure 5 Maps of site amplification factors for Fourier spectra (0.2Hz, 1Hz, 5Hz)

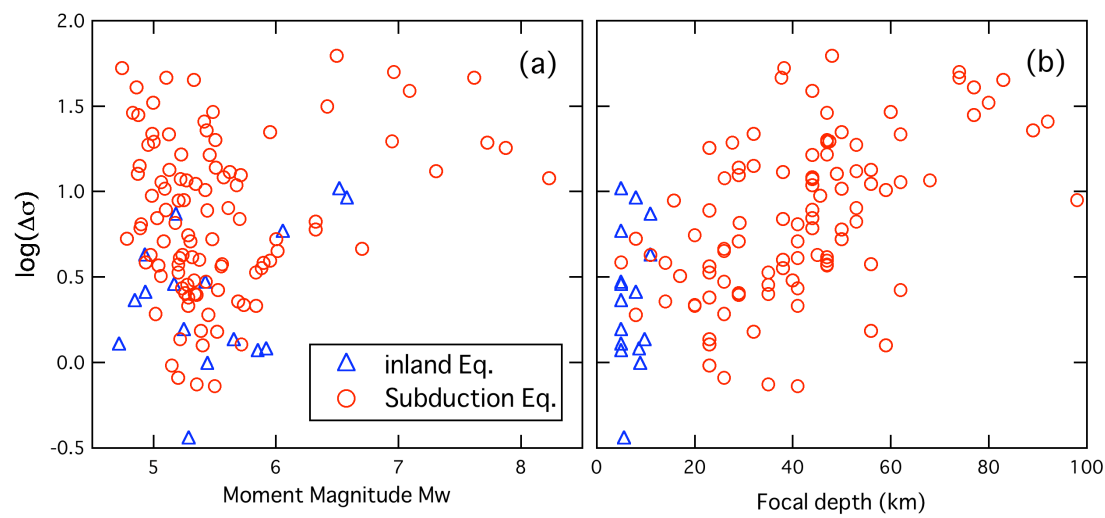


Figure 6 Stress drop versus moment magnitude and focal depth

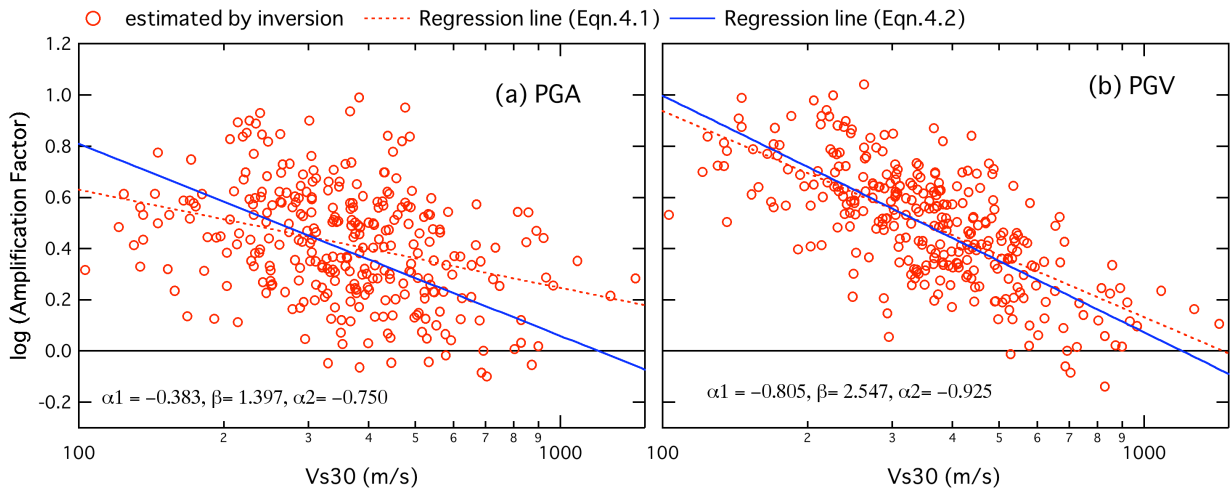


Figure 7 site amplification factors for PGA, PGV versus Vs30 (m/s)

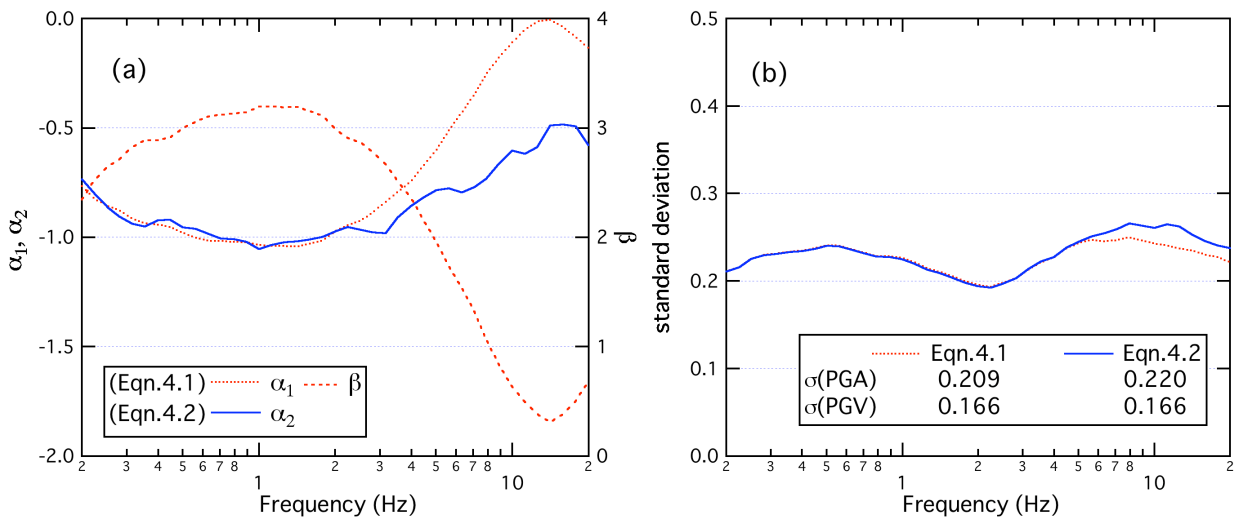


Figure 8 Regression parameters of site amplification factors for response spectra as a function of Vs30 (m/s)

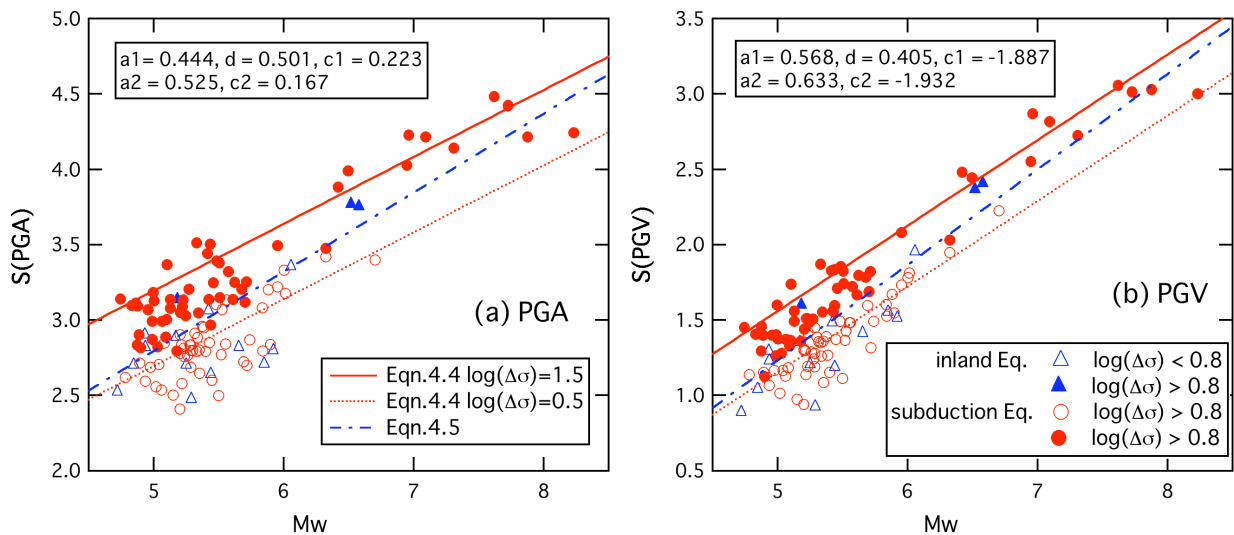


Figure 9 Relationships between earthquake terms for PGA, PGV and moment magnitude

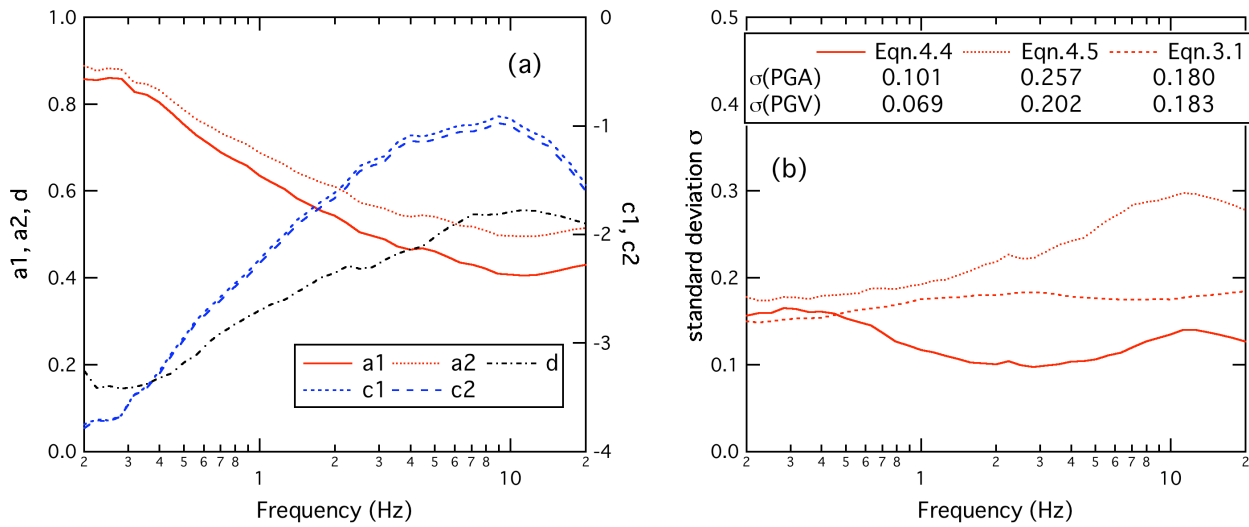


Figure 10 Regression coefficients and standard deviations of earthquake term for response spectra by Eqns.4.4-4.5

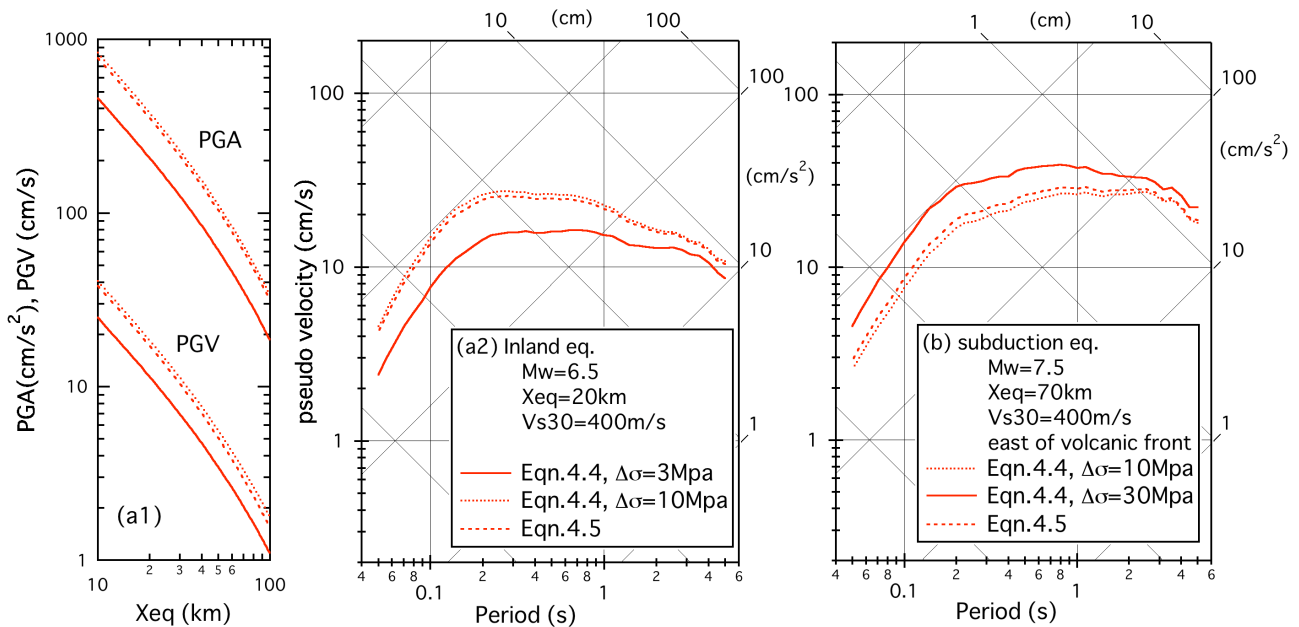


Figure 11 Estimation examples by the proposed GMPE.  
 (a1) (a2) M6.5 inland earthquake; (b) M7.5 subduction earthquake

Ohno, S., Ohta, T., Ikeura, T. and Takemura, M. (1993). Revision of Attenuation Formula Considering the Effect of Fault Size to Evaluate Strong Motion Spectra in Near Field. *Tectonophysics* **218**, 69-81.

Sato, R. (1989). Handbook of fault parameters for Japanese earthquakes, Kajima Institute Publishing Co. LTD.

Satoh, T. and Tatsumi, Y. (2002). Source, Path, and Site Effects for Crustal and Subduction Earthquakes Inferred from Strong Motion Records in Japan, *J. Struct. Constr. Eng., AIJ*, **556**, 15-24.

Takai, N and Okada, S. (2002). Improvement of Attenuation Formula of Earthquake Ground Motion in Consideration of the Volcanic Front, *Proc. of the The 11th Japan Earthquake Engineering Symposium*, 605-608.

Wessel, P. and W. H. F. Smith (1991). Free software helps map and display data, *EOS Trans. AGU*, **72**, 441.